

Rate-Splitting Multiple Access: The First Prototype and Experimental Validation of its Superiority over SDMA and NOMA

Xinze Lyu, *Student Member, IEEE*, Sundar Aditya, *Member, IEEE*, Junghoon Kim, *Member, IEEE* and Bruno Clerckx, *Fellow, IEEE*

Abstract—In multi-user multi-antenna communications, it is well-known in theory that Rate-Splitting Multiple Access (RSMA) can achieve a higher spectral efficiency than both Space Division Multiple Access (SDMA) and Non-Orthogonal Multiple Access (NOMA). However, an experimental evaluation of RSMA’s performance, relative to SDMA and NOMA, is missing in the literature, which is essential to address the ongoing debate between RSMA and NOMA over which is better suited to handle most efficiently the available resources and interference in 6G. In this paper, we address this critical knowledge gap by realizing the first-ever RSMA prototype using software-defined radios. Through measurements using our prototype, we empirically solve the modulation and coding scheme limited sum throughput maximization problem for RSMA, SDMA and NOMA for the two-user multiple-input single-output (MISO) scenario over (a) different pairs of line-of-sight channels that vary in terms of their relative pathloss and spatial correlation, and with (b) different channel state information quality. We observe that RSMA achieves the highest sum throughput across all these cases, whereas SDMA and NOMA are effective only in some cases. Furthermore, RSMA also achieves better fairness at a higher sum throughput than both SDMA and NOMA.

Index Terms—Rate-Splitting Multiple Access (RSMA), Space Division Multiple Access (SDMA), Non-Orthogonal Multiple Access (NOMA), RSMA prototyping, RSMA measurements, Software-defined Radio (SDR), RSMA for 6G.

I. INTRODUCTION

The evolutionary trajectory over successive generations of wireless networks has been towards achieving higher spectral efficiency, greater user fairness and higher energy efficiency. For upcoming 6G in particular, improvements in spectral and energy efficiency of at least 2x over 5G have been speculated [1]. To meet these targets, the underlying multiple access technique must be capable of offering higher efficiency, flexibility and coping with much higher levels of multi-user interference than Space Division Multiple Access (SDMA) – the state-of-the-art multiple access technique used in current wireless standards such as 3GPP 5G NR and IEEE 802.11. The two candidates widely believed to be capable of achieving

this in future wireless networks are Non-Orthogonal Multiple Access (NOMA) and Rate-Splitting Multiple Access (RSMA). We provide a brief description of each below, specifically focusing on practical implementations.

A. NOMA

NOMA is inspired by the fact that the capacity region of the K -user single-input-single-output (SISO) broadcast channel is achieved by superposition coding at the transmitter (TX) and successive interference cancellation (SIC) at the receivers (RXs) [2]. In SISO NOMA, users are ordered in decreasing order of their channel strength and the l -th strongest user decodes and subtracts the interference from the $K-l$ weaker users (i.e., SIC) before decoding its desired signal. The interference from the $l-1$ stronger users is treated as noise¹.

The optimality of NOMA for the SISO broadcast channel (in terms of achieving capacity) has been the driving force behind extensive investigations into NOMA for multiple-input-multiple-output (MIMO) systems with the aim of improving spectral efficiency [4], [5] and fairness [6] in 5G networks and beyond [7]. However, for the multi-antenna broadcast channel, NOMA is not optimal, in general, in a capacity-achieving sense [8]. This is because with multiple antennas at the TX, the spatial domain can be used to suppress interference without SIC at the RXs through either multi-user linear precoding (MU-LP) or non-linear precoding at the TX. MU-LP is the common approach adopted by SDMA [9]. Essentially, SDMA and NOMA represent two distinct interference management strategies; in SDMA, the interference is treated as noise, whereas in NOMA the interference from the weaker users is decoded by the stronger users [10]. Hence, NOMA provides substantial spectral efficiency gains over SDMA only when MU-LP cannot suppress the interference to near-noise levels. This occurs either in overloaded systems (i.e., more users than the number of antennas at the TX) or when the user channels in underloaded systems experience high spatial correlation. On the other hand, in non-overloaded systems where user channels do not experience high spatial correlation, NOMA can perform worse than SDMA [8]. While it can be argued that under high user density, groups of users with highly spatially correlated channels can be found with high probability, it does mean

¹This is commonly referred to as power-domain NOMA to distinguish it from other variants, such as code-domain and frequency-domain NOMA [3]. In this paper, NOMA refers only to power-domain NOMA.

This work was supported in part by UKRI Impact Acceleration Account (IAA) grant EP/X52556X/1.

X. Lyu, S. Aditya and B. Clerckx are with the Dept. of Electrical and Electronic Eng., Imperial College London, London SW7 2AZ, U.K. (e-mail: {x.lyu21, s.aditya, b.clerckx}@imperial.ac.uk). B. Clerckx is also with Silicon Austria Labs, 8010 Graz, Austria.

J. Kim is with the College of Ocean Science and Engineering, National Korea Maritime & Ocean University, Busan 49112, South Korea (e-mail: j.kim@kmou.ac.kr).

that MIMO-NOMA requires a user grouping strategy based on their channels, which has given rise to two approaches - beamforming-based and cluster-based NOMA [11].

NOMA Implementation

In terms of experimental evaluations, several papers have focussed on SISO-NOMA [12, Table 1]. MIMO-NOMA implementations are relatively fewer [13]–[15]. Link and system-level simulations were carried out in [13], along with measurements over emulated fading channels. Measurements involving over-the-air transmissions were carried out in [14], [15]. However, in these papers, the NOMA performance is compared with orthogonal multiple access instead of SDMA. To the best of our knowledge, no experimental comparison between NOMA and SDMA exists in the literature.

B. RSMA

Unlike NOMA with its SISO roots, RSMA was designed for multi-antenna communications from the outset. For the K -user multiple-input-single-output (MISO) case, RSMA produces $K+1$ data streams (i.e., channel-coded and modulated symbol streams) at the TX from the K user messages [16] (details in Section II-B). In contrast, both SDMA and NOMA generate K data streams. Similar to SDMA, each of the $K+1$ streams is linearly precoded (i.e., MU-LP) and transmitted over the air. At each RX, SIC is used (like NOMA) to decode *only two* streams to retrieve the desired message, regardless of a user's channel strength relative to the other users. Hence, unlike NOMA, no user grouping mechanism prior to data transmission is needed to realize spectral efficiency gains over SDMA.

RSMA's spectral efficiency gains over SDMA and NOMA stem from the fact that it is degrees-of-freedom (DoF) optimal under perfect and imperfect channel state information (CSI) [8], [16]. Furthermore, RSMA has also been shown, in theory, to achieve spectral efficiency gains over SDMA and NOMA under varying interference levels, network loads and user deployments [10]. Apart from spectral efficiency, RSMA has also been shown to achieve – again, in theory – performance improvements over SDMA and NOMA in terms of other metrics such as energy efficiency, fairness, mixed-critical quality-of-service and tight latency requirements, etc. (see [17], [18] and the references therein for a comprehensive survey). These performance improvements stem from RSMA's unique interference mitigation strategy, wherein at each user, the interference is *partially decoded and partially treated as noise*. In doing so, RSMA generalizes both SDMA and NOMA [10], [19]. Taken together, all of these features make RSMA an attractive candidate for physical layer multiple access in 6G, provided the promised gains can be demonstrated in practice. In particular, an experimental comparison between RSMA, SDMA and NOMA is needed as a starting point to address the pressing question of which multiple access technique is best equipped to deliver the spectral efficiency enhancements expected from 6G.

RSMA Implementation

Despite its impressive benefits, the practical implementation of RSMA is still in its infancy, with the state-of-the-art focusing on the closely related issues of erroneous SIC, receiver design, finite constellation and adaptive modulation and coding (AMC) for RSMA to minimize the block error rate due to the combined effects of imperfect/outdated CSI at the TX (CSIT) and finite blocklength [20]–[24]. Among these, RSMA link-level simulations were conducted in [20]–[22], feedback-based RSMA link adaptation was investigated in [23], while [24] considered a flexible variant of RSMA, where only a subset of the receivers employ SIC. Though important, these practical aspects have also been tackled only through theory/simulations, and no experimental verification of RSMA's benefits has been reported till date.

In this paper, we address this critical knowledge gap by realizing the first-ever RSMA prototype using software-defined radios (SDRs). Using our prototype, we experimentally compare the throughput and fairness performance of RSMA, SDMA and NOMA. Our contributions are as follows:

- We implement RSMA on SDRs using a two-stage protocol. In Stage 1, orthogonal pilot signals are transmitted by the TX for CSI estimation at each RX. The estimated CSI is then fed back to the TX, either unquantized or quantized to emulate perfect and imperfect CSIT, respectively (Section II-A). The CSIT is used to design the precoded RSMA signal that is transmitted in Stage 2 (Section II-B). We use OFDM signals largely based on IEEE 802.11g physical layer frames to implement the data payload in the RSMA signal (Section III). The above two-stage protocol can also be used to implement SDMA and NOMA in our prototype with appropriate changes to Stage 2.
- For the two-user MISO scenario, we formulate the practically relevant *modulation and coding scheme (MCS)-limited sum throughput maximization problem* for RSMA, and establish its relationship to the canonical sum rate maximization problem that is widely analyzed in theory (Section II-B). The MCS-limited sum throughput maximization problem can also be formulated for SDMA and NOMA (Table I).
- Through measurements using our prototype, we empirically solve the MCS-limited sum throughput maximization problem for RSMA, SDMA and NOMA for the two-user MISO scenario over line-of-sight channels in a lab environment, where the pair of channels differ in terms of their relative strength and spatial correlation (Section IV). We empirically observe that
 - With unquantized CSI feedback, NOMA achieves significant throughput gains over SDMA when channels have high spatial correlation. On the other hand, when the channels have low spatial correlation, the SDMA throughput is higher than NOMA. RSMA, however, achieves the highest throughput not only under either extreme but also over channels that lie in between w.r.t their spatial correlation. These outcomes are consistent with theoretical predictions

in [10], [19].

- With quantized CSI feedback, NOMA achieves significant throughput gains over SDMA even with channels having low spatial correlation, provided there is a sufficiently large disparity between the channel strengths. The NOMA throughput performance is also at par with that of RSMA under these conditions. Essentially, the imperfect CSI disproportionately diminishes the weaker user's throughput for SDMA, whereas both RSMA and NOMA provide higher throughput to the weaker user via the common stream (see Section II-B for definition). However, when the channel strength disparity is not sufficiently large, RSMA achieves throughput gains over NOMA as well. These outcomes are consistent with theoretical predictions in [8], [17], [18].
- With both quantized and unquantized CSI feedback, RSMA achieves better fairness at higher throughputs than both SDMA and NOMA. This too is consistent with theoretical predictions in [8], [17], [18].

C. Organization

The rest of this paper is organized as follows. In Section II, we introduce the RSMA system model for the two-user MISO scenario and formulate the practically relevant MCS-limited sum throughput maximization problem. In Section III, we provide a detailed description of our SDR-based RSMA implementation. In Section IV, we empirically solve the MCS-limited sum throughput maximization problem for RSMA, SDMA and NOMA through measurements using our prototype and compare the sum throughput and fairness performance of the three schemes. Finally, Section V concludes the paper.

D. Notation

Column vectors are represented using lowercase bold letters (e.g., \mathbf{x}). $(\cdot)^H, \|\cdot\|, \cup$ and \emptyset denote the Hermitian operator, the Euclidean norm, the union operation and the empty set, respectively. $\text{Re}(\cdot)$ and $\text{Im}(\cdot)$ denote the real and imaginary parts of a complex number, $\lfloor \cdot \rfloor$ denotes the floor function, and $\mathcal{CN}(0, \sigma^2)$ denotes the circularly symmetric complex Gaussian distribution with zero mean and variance σ^2 .

II. SYSTEM MODEL

Consider a two-antenna TX communicating with two single-antenna users/RXs, using OFDM² signals over N_c subcarriers. The communications takes place over two stages.

- **Stage 1:** First, the TX transmits orthogonal pilot signals for channel estimation at the RXs. The estimated CSI is then fed back to the TX through a separate link.
- **Stage 2:** Using the CSI acquired in Stage 1, the TX designs the precoder and the transmit signal to maximize the sum throughput.

We describe each stage, in turn, in Sections II-A and II-B.

²In principle, RSMA can be used with any waveform. Our choice of OFDM is motivated by its prevalence in modern communications systems. However, in the context of 6G, alternatives to OFDM, such as OTFS have received considerable attention. RSMA for such waveforms – especially experimental evaluations – is a relevant topic yet to be investigated.

A. Stage 1: Channel Model and CSI feedback

Let $\mathbf{h}_i[k] := [h_{i1}[k], h_{i2}[k]]^T \in \mathbb{C}^{2 \times 1}$ denote the true frequency flat, slowly varying channel between the TX and RX i ($i = 1, 2$) over the k -th subcarrier ($k = 0, \dots, N_c - 1$). Similarly, let $\hat{\mathbf{h}}_i[k]$ denote the estimate of $\mathbf{h}_i[k]$, obtained at RX i through pilot signals transmitted by the TX. To reduce feedback overhead, let $\hat{\mathbf{h}}_i$ denote the *wideband CSI* evaluated at RX i by averaging $\hat{\mathbf{h}}_i[k]$ over the subcarriers, i.e.,

$$\hat{\mathbf{h}}_i := \frac{1}{N_c} \sum_{k=0}^{N_c-1} \hat{\mathbf{h}}_i[k], \quad (i = 1, 2). \quad (1)$$

For CSI feedback of $\hat{\mathbf{h}}_i$ from RX i to the TX in our experiments, we consider two cases to emulate perfect and imperfect CSI at the TX.

- **Unquantized feedback:** Let $\hat{\mathbf{h}}_i^{\text{UQ}} = [\hat{h}_{i1}^{\text{UQ}} \hat{h}_{i2}^{\text{UQ}}]$ denote the unquantized version of $\hat{\mathbf{h}}_i$, where each complex \hat{h}_{il}^{UQ} ($i, l \in \{1, 2\}$) is a 128-bit representation of \hat{h}_{il} (i.e., a 64-bit double-precision floating-point number for the real and imaginary parts). This is intended to emulate perfect CSI at the TX.
- **Quantized feedback:** Let $\hat{\mathbf{h}}_i^{\text{Q}} = [\hat{h}_{i1}^{\text{Q}} \hat{h}_{i2}^{\text{Q}}]$ denote the quantized version of $\hat{\mathbf{h}}_i$, where each complex \hat{h}_{il}^{Q} ($i, l \in \{1, 2\}$) is an 8-bit representation of \hat{h}_{il} (i.e., 4 bits for the real and imaginary parts). The quantization mechanism is described in Appendix A, and is based on based on IEEE 802.11n [25]. It results in a more than 90% reduction in the CSI feedback overhead, and is intended to emulate imperfect CSI at the TX.

The feedback CSI is used by the TX to design the precoders, as described in the following subsection.

B. Stage 2: RSMA Signal Design

For the two-user MISO scenario, Fig. 1 depicts RSMA in operation. Let W_1 and W_2 denote the messages corresponding to RX 1 and RX 2, respectively. At the TX, each W_i ($i = 1, 2$) is split into common and private portions – denoted by $W_{c,i}$ and $W_{p,i}$, respectively – by the message splitter. The common portions of each RX's message (i.e., $W_{c,1}$ and $W_{c,2}$) are combined into a common message, which is then encoded and modulated to form a common stream, $s_c[k]$ ($k = 0, \dots, N_c - 1$) over the subcarriers. On the other hand, the private portions of RX i 's message are individually encoded and modulated to form private streams, $s_i[k]$. All three streams (i.e., $s_c[k]$, $s_1[k]$ and $s_2[k]$) are linearly precoded to form the transmit OFDM frequency domain signal as follows:

$$\mathbf{x}[k] = \mathbf{p}_c s_c[k] + \mathbf{p}_1 s_1[k] + \mathbf{p}_2 s_2[k] \quad (k = 0, \dots, N_c - 1), \quad (2)$$

where \mathbf{p}_c is referred to as the common stream precoder, and \mathbf{p}_i the private stream precoder of RX i .

After appropriate DFT-based processing, the received OFDM frequency domain signal, $y_i[k]$, at RX i is given by:

$$\begin{aligned} y_i[k] &= \mathbf{h}_i^H[k] \mathbf{x}[k] + n_i[k], \quad (k = 0, \dots, N_c - 1) \\ &= \mathbf{h}_i^H[k] \mathbf{p}_c s_c[k] + \mathbf{h}_i^H[k] \mathbf{p}_1 s_1[k] + \mathbf{h}_i^H[k] \mathbf{p}_2 s_2[k] \\ &\quad + n_i[k] \quad (i = 1, 2), \end{aligned} \quad (3)$$

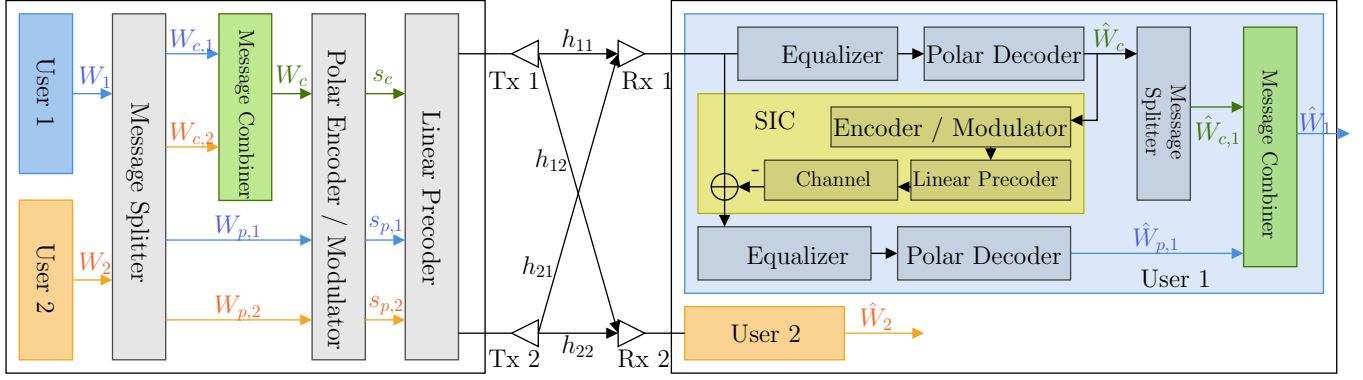


Fig. 1: RSMA block diagram for the two-user MISO scenario.

where $n_i[k] \sim \mathcal{CN}(0, \sigma^2)$ is the thermal noise. We assume that precoded pilot signals have been interspersed in some of the subcarriers of $\mathbf{x}[k]$ to help RX i estimate $\mathbf{h}_i^H[k]\mathbf{p}_c$ and $\mathbf{h}_i^H[k]\mathbf{p}_i$ upon receiving $y_i[k]$ ³. Then, after suitable equalization (e.g., MMSE), RX i first decodes $s_c[k]$ to recover W_c , while treating the interference from the $s_1[k]$ and $s_2[k]$ as noise. The decoded estimate of W_c at RX i , denoted by $\hat{W}_c^{(i)}$, is simultaneously sent to:

- the message splitter to extract $\hat{W}_{c,i}^{(i)}$ – the portion of $\hat{W}_c^{(i)}$ containing data meant for RX i 's, and
- the SIC module, which generates an estimate of $\mathbf{h}_i^H[k]\mathbf{p}_c s_c[k]$ and subtracts it from $y_i[k]$. The residue is once again subjected to equalization, this time to decode $s_i[k]$ by treating the interference from the other private stream as noise. Let $\hat{W}_{p,i}$ denote the decoded estimate of $W_{p,i}$ at RX i .

Let $\mathbf{P} = [\mathbf{p}_c \ \mathbf{p}_1 \ \mathbf{p}_2]$. As a function of \mathbf{P} , from (3), the achievable rate (in bits/s/Hz) for error-free decoding of $s_c[k]$ at RX i , denoted by $R_{c,i}(\mathbf{P})$, is given by:

$$R_{c,i}(\mathbf{P}) = \min_k \log_2 \left(1 + \frac{|\mathbf{h}_i^H[k]\mathbf{p}_c|^2}{\sigma^2 + |\mathbf{h}_i^H[k]\mathbf{p}_1|^2 + |\mathbf{h}_i^H[k]\mathbf{p}_2|^2} \right), \quad (4)$$

where the minimum over k arises because the encoded and modulated common stream is embedded over subcarriers in the frequency domain. Additionally, since both RXs must first decode $s_c[k]$, it follows that the achievable rate for error-free decoding of $s_c[k]$ at both RXs, denoted by $R_c(\mathbf{P})$, is given by:

$$R_c(\mathbf{P}) = \min(R_{c,1}(\mathbf{P}), R_{c,2}(\mathbf{P})). \quad (5)$$

Assuming perfect SIC operation, the achievable rate for error-free decoding of $s_i[k]$ at RX i , similar to (4), is given by:

$$R_i(\mathbf{P}) = \min_k \log_2 \left(1 + \frac{|\mathbf{h}_i^H[k]\mathbf{p}_i|^2}{\sigma^2 + |\mathbf{h}_i^H[k]\mathbf{p}_j|^2} \right), \quad j \neq i. \quad (6)$$

Thus, the achievable rate at RX i for error-free recovery of W_i , denoted by $R_i^{\text{RSMA}}(\mathbf{P})$ is given by:

$$R_i^{\text{RSMA}}(\mathbf{P}) = (W_{c,i}/W_c)R_c(\mathbf{P}) + R_i(\mathbf{P}) \quad (7)$$

³These pilots play a role similar to the demodulation reference signals (DM-RS) used in LTE and 5G NR.

where the first term captures the fraction of the common message, W_c , intended for RX i . Consequently, the achievable RSMA sum rate, denoted by $R^{\text{RSMA}}(\mathbf{P})$, is:

$$\begin{aligned} R^{\text{RSMA}}(\mathbf{P}) &= R_1^{\text{RSMA}}(\mathbf{P}) + R_2^{\text{RSMA}}(\mathbf{P}) \\ &= R_c(\mathbf{P}) + R_1(\mathbf{P}) + R_2(\mathbf{P}) \end{aligned} \quad (8)$$

The canonical *sum rate maximization problem*, where the precoders at the TX are optimized to maximize $R^{\text{RSMA}}(\mathbf{P})$ is formulated as follows:

$$OP_{\text{sr}}^{\text{RSMA}} : \max_{\mathbf{P}} R^{\text{RSMA}}(\mathbf{P}) \quad (9)$$

$$\text{s.t. } \text{tr}(\mathbf{P}\mathbf{P}^H) \leq P_t, \quad (10)$$

where (10) restricts the transmit power to P_t . Through the well-known Rate-WMMSE relationship [26], the non-convex problem in $OP_{\text{sr}}^{\text{RSMA}}$ can be transformed into a sequence of tractable sub-problems that can be iteratively solved till convergence to a local optimum. This is commonly known in the literature as the *WMMSE method* and despite only guaranteeing local optimality, it is widely recognized as a benchmark solution for the family of MIMO precoder design problems, of which $OP_{\text{sr}}^{\text{RSMA}}$ is a specific instance corresponding to RSMA. Let $\mathbf{P}_{\text{wmmse}}^{\text{RSMA}}$ denote the precoders obtained by applying the WMMSE method to solve $OP_{\text{sr}}^{\text{RSMA}}$.

Remark 1 (Imperfect CSI at the TX). $OP_{\text{sr}}^{\text{RSMA}}$ contains a slight abuse of notation for the sake of simplicity. Let $\hat{\mathbf{H}}^{\text{TX}} := [\hat{\mathbf{h}}_1^{\text{TX}} \ \hat{\mathbf{h}}_2^{\text{TX}}]$ denote the CSIT, where $\hat{\mathbf{h}}_i^{\text{TX}} \in \{\hat{\mathbf{h}}_i^{\text{UQ}}, \hat{\mathbf{h}}_i^{\text{QI}}\}$, as described in Section II-A. Strictly speaking, to obtain the objective function of $OP_{\text{sr}}^{\text{RSMA}}$ at the TX, $\mathbf{h}_i[k]$ in (4) and (6) should be replaced by $\hat{\mathbf{h}}_i^{\text{TX}}$, so that the solution to $OP_{\text{sr}}^{\text{RSMA}}$ becomes a function of the CSIT.

In this paper, the main performance metric in our measurements is the throughput (measured in bits/s). Over an effective bandwidth⁴, B , the achievable RSMA sum throughput, denoted by $T^{\text{RSMA}}(\mathbf{P})$, is related to $R^{\text{RSMA}}(\mathbf{P})$ in (8) via $T^{\text{RSMA}}(\mathbf{P}) = BR^{\text{RSMA}}(\mathbf{P})$. Hence, it follows that $T^{\text{RSMA}}(\mathbf{P}_{\text{wmmse}}^{\text{RSMA}})$ is a good benchmark in terms of the

⁴The effective bandwidth is the portion of the total bandwidth available for data transfer, after accounting for signaling overheads (e.g., cyclic prefix in the case of OFDM).

maximum achievable RSMA sum throughput. However, this benchmark is hard to realize in practice because:

1. In state-of-the-art communications systems, PHY layer transmissions are restricted to a finite collection of modulation and coding scheme (MCS) levels (e.g., QPSK, rate 1/2), which caps the maximum achievable sum throughput, and
2. Error-free decoding of the transmitted messages at the RX cannot be guaranteed due to finite block length effects, which further diminishes the realized throughput.

We address these two points by first characterizing the *MCS-limited* throughput. An MCS level can be defined by a pair (m, r) , where positive integer m denotes the bits per constellation symbol (e.g., 2 for QPSK) and $r \in (0, 1]$ denotes the code rate. Hence, the achievable rate (in bits/s/Hz) for MCS level (m, r) equals mr , and the achievable throughput is Bmr . Let (m_c, r_c) , (m_1, r_1) and (m_2, r_2) denote the MCS levels chosen for $s_c[k]$, $s_1[k]$ and $s_2[k]$, respectively. Then, the *MCS-limited* RSMA sum throughput, denoted by $T_{\text{mcs}}^{\text{RSMA}}(\mathbf{P}, \mathcal{M})$, is given by:

$$\begin{aligned} T_{\text{mcs}}^{\text{RSMA}}(\mathbf{P}, \mathcal{M}) &= Bm_c r_c(\mathbf{p}_c) \times \mathbb{P}(\hat{W}_c^{(1)} = W_c; \hat{W}_c^{(2)} = W_c) \\ &\quad + Bm_1 r_1(\mathbf{p}_1) \times \mathbb{P}(\hat{W}_{p,1} = W_{p,1}) \\ &\quad + Bm_2 r_2(\mathbf{p}_2) \times \mathbb{P}(\hat{W}_{p,2} = W_{p,2}). \end{aligned} \quad (11)$$

The RHS of (11) indicates that the MCS levels of the streams are, in general, a function of the corresponding precoders. The probability terms capture the loss in throughput due to decoding errors – specifically, $\mathbb{P}(\hat{W}_c^{(1)} = W_c; \hat{W}_c^{(2)} = W_c)$ denotes the probability that W_c is correctly decoded at both RXs, while $\mathbb{P}(\hat{W}_{p,i} = W_{p,i})$ denotes the probability that $W_{p,i}$ is correctly decoded at RX i . Thus, similar to $OP_{\text{sr}}^{\text{RSMA}}$ in (9)-(10), the *MCS-limited RSMA sum throughput maximization problem*, which is of considerable practical relevance, can be defined as follows:

$$OP_{\text{mcs}}^{\text{RSMA}} : \max_{\mathbf{P}, \mathcal{M}} T_{\text{mcs}}^{\text{RSMA}}(\mathbf{P}_{\text{wmmse}}^{\text{RSMA}}, \mathcal{M}) \quad (12)$$

$$\mathcal{M} \in \mathbb{M}, \quad (13)$$

where \mathbb{M} denotes the collection of permissible MCS levels for the three streams, which is typically pre-determined through standards (see Table III for the \mathbb{M} used in our measurements). $OP_{\text{mcs}}^{\text{RSMA}}$ does not have a closed form solution, as the message decoding probabilities in (11) are difficult to characterize in terms of $\mathbf{P}_{\text{wmmse}}^{\text{RSMA}}$ and \mathcal{M} . However, these probabilities can be empirically evaluated through measurements. This motivates us to empirically solve $OP_{\text{mcs}}^{\text{RSMA}}$ through a brute force search⁵ over \mathbb{M} , which is the focus of our measurements in Section IV using our SDR-based RSMA prototype. We conclude this subsection with the following remark:

Remark 2 (Wideband precoders). *In principle, narrowband precoders for each subcarrier (i.e., $\mathbf{p}_c[k]$, $\mathbf{p}_1[k]$, $\mathbf{p}_2[k]$: $k = 0, \dots, N_c - 1$) could increase the achievable rate in (4)-(8) by adapting to channel variations at subcarrier-level granularity.*

⁵A more sophisticated empirical approach involves link adaptation, where the most suitable MCS level is determined by an ARQ-based mechanism [23]. This is left for future work.

However, this would involve huge signalling overhead in both directions, as: (a) narrowband CSI (i.e., $\hat{\mathbf{h}}_i[k]$ for several, if not all, k) would need to be fed back to the TX for precoder design, and (b) more demodulation reference signals would have to be embedded in the transmit signal to estimate $\mathbf{h}_i^H[k]\mathbf{p}_c[k]$ and $\mathbf{h}_i^H[k]\mathbf{p}_i[k]$ at RX i for all k . Thus, to reduce the signalling overhead, we assume the same precoders, \mathbf{P} , across all the subcarriers.

C. RSMA v/s SDMA v/s NOMA

In general, the splitting of the user messages in Fig. 1 need not be equal (i.e., 50-50) between the common and private portions, nor does the ratio between the common and private portions need to be fixed across both messages. In fact, SDMA and NOMA are special cases of RSMA corresponding to specific choices of message splitting, as explained in the following remarks.

Remark 3 (SDMA as a special case of RSMA). *For the special case where the common stream is turned off – i.e., $W_i = W_{p,i}$ ($i = 1, 2$) in Fig. 1 – RSMA reduces to SDMA [19].*

Remark 4 (NOMA as a special case of RSMA). *Without loss of generality, suppose RX 2 has a weaker channel than RX 1. For the special case where the private stream of RX 2 is turned off, and no portion of W_1 is allocated to the common stream – i.e., $W_1 = W_{p,1}$, $W_2 = W_{c,2} = W_c$ in Fig. 1 – RSMA reduces to NOMA [19].*

This flexibility in message splitting provided by RSMA characterizes its interference management philosophy, as follows:

- **SDMA**: In the absence of a common stream, the interference experienced at RX i due to W_j ($j \neq i$) is treated as noise.
- **NOMA**: The common stream allows the stronger RX 1 to fully decode and subtract the interference it experiences (from W_2). The weaker RX 2 continues to treat the interference it experiences (from W_1) as noise, like SDMA.
- **RSMA**: The interference at RX i due to W_j ($j \neq i$) is *partially decoded* ($W_{c,j}$) and *partially treated as noise* ($W_{p,j}$). This feature enables RSMA to softly bridge between SDMA and NOMA [10], [19]. In other words, when the two channels are orthogonal, the optimal solution to $OP_{\text{sr}}^{\text{RSMA}}$ in (9)-(10) coincides with SDMA. Similarly, when the channels are aligned and one of them is much stronger than the other, the optimal solution to $OP_{\text{sr}}^{\text{RSMA}}$ reduces to NOMA. Importantly, over the vast majority of channels that do not fall in either extreme, RSMA is expected to provide significant gains over both SDMA and NOMA, which we aim to demonstrate experimentally in Section IV.

Based on Remarks 3 and 4, the expressions corresponding to SDMA and NOMA in (2)-(13) can be obtained by discarding \mathbf{p}_c (SDMA) and \mathbf{p}_2 (NOMA). These expressions are provided in Table I for clarity. In Sections IV-B and IV-C, we provide an experimental RSMA v/s SDMA v/s NOMA

performance comparison by empirically solving OP_{mcs}^{ma} , $ma \in \{\text{RSMA}, \text{SDMA}, \text{NOMA}\}$ using our SDR-based RSMA prototype. In the following section, we present details of our prototype, as well as how the system model described above in Sections II-A and II-B is implemented.

III. RSMA PROTOTYPE USING SDR

A. Hardware setup

Our RSMA prototype is built using National Instruments' (NI) Universal Software Radio Peripherals (USRPs). As shown in Fig. 2, two USRP-2942 units are used to realize the two-user MISO scenario. In particular, the RX antennas (TP-LINK TL-ANT2405C) are connected to its USRP using coaxial cables, which allows them to be moved to create different channel configurations (Fig. 4). The USRPs share a common timing source (CDA-2990), and are connected to a workstation through which they are controlled using LabVIEW NXG. All connections are through PCIe cables, facilitated by a PCIe bus (CPS-8910). The total transmit power, P_t , is 23dBm. A list of hardware components is provided in Table II.

B. RSMA Implementation Details

The USRPs are capable of operating in the 2.4GHz ISM band. Hence, we choose a center frequency of 2.484GHz for our transmissions⁶. For ease of practicalities like synchronization and channel estimation, it is convenient to implement signals based on well-known physical layer standards (e.g., IEEE 802.11 frames) in a prototype. Hence, we adopt several features of the IEEE 802.11g physical layer frames in our signal design. Next, we describe in detail how Stages 1 and 2 from Sections II-A and II-B, respectively, are implemented in our prototype:

a) Stage 1: Each TX antenna transmits a pilot signal orthogonally in time comprising a Short Training Field (STF, $8\mu\text{s}$ in duration) and a Long Training Field (LTF, $8\mu\text{s}$ in duration), as shown in the top portion of Fig. 3. The STF is used for synchronization and coarse frequency offset estimation, while the LTF is used to obtain a least squares estimate of the CSI at each RX over all the subcarriers (i.e., $\hat{\mathbf{h}}_i[k]$ in Section II-A).

b) Stage 2: Here, the transmitted signal consists of a preamble followed by the data payload, as shown in the middle portion of Fig. 3.

- **Preamble:** The preamble consists of one STF and three LTFs. The function of the STF is the same as the first stage, while the LTFs are precoded in order to estimate the *precoded CSI* for equalization at the RX; in particular, the first LTF is used to estimate $\mathbf{h}_i^H \mathbf{p}_c$ at RX i ($i = 1, 2$) for decoding the common stream, the second to estimate $\mathbf{h}_1^H \mathbf{p}_1$ to decode the private stream meant for RX 1, and the third to estimate $\mathbf{h}_2^H \mathbf{p}_2$ to decode the private stream meant for RX 2.

- **Data Payload:** For the payload, we use OFDM signals over a total bandwidth of 20MHz with $N_c = 64$ subcarriers (labeled DATA in Fig. 3) and a cyclic prefix (CP)

of 16 samples per OFDM symbol. Aligned with IEEE 802.11 frames, 52 subcarriers are used for communications while the rest serve as guard bands. Among these 52 subcarriers, 48 are used to carry data symbols, with the remaining used for fine phase shifting (FPS)⁷. This yields an effective bandwidth of:

$$B = 20\text{MHz} \times \underbrace{(64/80)}_{\text{CP overhead}} \times \underbrace{(48/64)}_{\text{Guard band overhead}} = 12\text{MHz} \quad (14)$$

The payload consists of three superposed streams (one common, two private), each comprising 50 OFDM symbols (labeled DATA 1 through DATA 50, as shown in the bottom portion of Fig. 3).

- **MCS Implementation:** Table III lists the MCS levels, \mathbb{M} , implemented in our prototype. MCS indices 0 through 7 are identical to IEEE 802.11g, where 64-QAM is the largest supported constellation. To allow for the possibility of higher data rates due to RSMA's enhanced interference suppression, we implement two more MCS levels supporting 256-QAM (MCS indices 8 and 9). After the preamble, the first OFDM symbol (labelled SERVICE in the bottom portion of Fig. 3) contains the MCS information of each stream.

Unlike the IEEE 802.11 family of standards, which uses LDPC codes for error correction, we implement Polar codes augmented with an 8-bit cyclic redundancy check [29], [30], along with successive cancellation list decoding [31], with a list depth of 2.

An instance of Stage 1 and Stage 2, as described above and illustrated in Fig. 3, constitutes a single measurement run. To empirically solve OP_{mcs}^{ma} ($ma \in \{\text{RSMA}, \text{SDMA}, \text{NOMA}\}$) from Table I, we conduct 100 measurement runs. Let $D_{s,c}^{ma}$ denote the number of runs in which the common stream is successfully decoded by both RXs. Similarly, let $D_{s,i}^{ma}$ ($i = 1, 2$) denote the number of runs in which RX i successfully decodes its private stream. Consider the expressions for the MCS-limited sum throughput in Table I (third last row). Replacing the decoding probabilities therein with their empirical estimates, the *measured* sum throughput for each multiple access scheme is given by:

$$T_{mcs}^{\text{RSMA}}(\mathbf{P}_{\text{wmmse}}^{\text{RSMA}}, \mathcal{M}) = \frac{D_{s,c}^{\text{RSMA}}}{100} B m_c r_c + \sum_{i=1}^2 \frac{D_{s,i}^{\text{RSMA}}}{100} B m_i r_i \quad (15)$$

$$T_{mcs}^{\text{SDMA}}(\mathbf{P}_{\text{wmmse}}^{\text{SDMA}}, \mathcal{M}) = \frac{D_{s,1}^{\text{SDMA}}}{100} B m_1 r_1 + \frac{D_{s,2}^{\text{SDMA}}}{100} B m_1 r_1 \quad (16)$$

$$T_{mcs}^{\text{NOMA}}(\mathbf{P}_{\text{wmmse}}^{\text{NOMA}}, \mathcal{M}) = \frac{D_{s,c}^{\text{NOMA}}}{100} B m_c r_c + \frac{D_{s,1}^{\text{NOMA}}}{100} B m_1 r_1, \quad (17)$$

where B is given by (14) and the MCS levels are chosen from Table III.

⁶This corresponds to channel no. 14 in the IEEE 802.11 family of standards for the 2.4GHz band. We use this channel to avoid ambient WiFi interference, as it is not commercially used in the UK.

⁷FPS is used to correct the common phase error across all subcarriers in one OFDM symbol [28].

Quantity	Expression	
Message splitting	$W_i = W_{c,i} \cup W_{p,i} \ (i = 1, 2)$ $W_c = W_{c,1} \cup W_{c,2}$ RSMA: $W_{c,i}, W_{p,i} \neq \emptyset$, in general SDMA: $W_{c,i} = \emptyset, W_{p,i} = W_i$ NOMA: $W_{c,1} = \emptyset, W_{p,1} = W_1$ and $W_{c,2} = W_2, W_{p,2} = \emptyset$	
Precoders	RSMA:	$\mathbf{P} = [\mathbf{p}_c \ \mathbf{p}_1 \ \mathbf{p}_2]$
	SDMA:	$\mathbf{P} = [\mathbf{p}_1 \ \mathbf{p}_2]$
	NOMA:	$\mathbf{P} = [\mathbf{p}_c \ \mathbf{p}_1]$
Achievable common stream rate at RX i	RSMA:	$R_{c,i}(\mathbf{P}) = \min_k \log_2 \left(1 + \frac{ \mathbf{h}_i^H[k] \mathbf{p}_c ^2}{\sigma^2 + \mathbf{h}_i^H[k] \mathbf{p}_1 ^2 + \mathbf{h}_i^H[k] \mathbf{p}_2 ^2} \right)$ $R_c(\mathbf{P}) = \min_i R_{c,i}(\mathbf{P})$
	SDMA:	$R_{c,i}(\mathbf{P}) = R_c(\mathbf{P}) = 0$
	NOMA:	$R_{c,i}(\mathbf{P}) = \min_k \log_2 \left(1 + \frac{ \mathbf{h}_i^H[k] \mathbf{p}_c ^2}{\sigma^2 + \mathbf{h}_i^H[k] \mathbf{p}_1 ^2} \right)$ $R_c(\mathbf{P}) = \min_i R_{c,i}(\mathbf{P})$
Achievable pvt. stream rate at RX i	RSMA:	$R_i(\mathbf{P}) = \min_k \log_2 \left(1 + \frac{ \mathbf{h}_i^H[k] \mathbf{p}_i ^2}{\sigma^2 + \mathbf{h}_i^H[k] \mathbf{p}_j ^2} \right) \ (j \neq i)$
	SDMA:	$R_i(\mathbf{P}) = \min_k \log_2 \left(1 + \frac{ \mathbf{h}_i^H[k] \mathbf{p}_i ^2}{\sigma^2 + \mathbf{h}_i^H[k] \mathbf{p}_j ^2} \right) \ (j \neq i)$
	NOMA:	$R_1(\mathbf{P}) = \min_k \log \left(1 + \frac{ \mathbf{h}_1^H[k] \mathbf{p}_1 ^2}{\sigma^2} \right)$ $R_2(\mathbf{P}) = 0$
Achievable sum rate	RSMA:	$R^{\text{RSMA}}(\mathbf{P}) = R_c(\mathbf{P}) + R_1(\mathbf{P}) + R_2(\mathbf{P})$
	SDMA:	$R^{\text{SDMA}}(\mathbf{P}) = R_1(\mathbf{P}) + R_2(\mathbf{P})$
	NOMA:	$R^{\text{NOMA}}(\mathbf{P}) = R_c(\mathbf{P}) + R_1(\mathbf{P})$
Sum rate max. problem	$OP_{\text{sr}}^{\text{ma}} : \max_{\mathbf{P}} R^{\text{ma}}(\mathbf{P})$ s.t. $\text{tr}(\mathbf{P}\mathbf{P}^H) \leq P_t$	
Achievable sum throughput	$T^{\text{ma}}(\mathbf{P}) = BR^{\text{ma}}(\mathbf{P})$, where $\text{ma} \in \{\text{RSMA}, \text{SDMA}, \text{NOMA}\}$	
MCS levels	RSMA:	$\mathcal{M} = \{(m_c, r_c), (m_1, r_1), (m_2, r_2)\}$
	SDMA:	$\mathcal{M} = \{(m_1, r_1), (m_2, r_2)\}$
	NOMA:	$\mathcal{M} = \{(m_c, r_c), (m_1, r_1)\}$
MCS-limited sum rate	RSMA:	$R_{\text{mcs}}^{\text{RSMA}}(\mathbf{P}, \mathcal{M}) = m_c r_c(\mathbf{p}_c) + m_1 r_1(\mathbf{p}_1) + m_2 r_2(\mathbf{p}_2)$
	SDMA:	$R_{\text{mcs}}^{\text{SDMA}}(\mathbf{P}, \mathcal{M}) = m_1 r_1(\mathbf{p}_1) + m_2 r_2(\mathbf{p}_2)$
	NOMA:	$R_{\text{mcs}}^{\text{NOMA}}(\mathbf{P}, \mathcal{M}) = m_c r_c(\mathbf{p}_c) + m_1 r_1(\mathbf{p}_1)$
MCS-limited sum throughput	RSMA:	$T_{\text{mcs}}^{\text{RSMA}}(\mathbf{P}, \mathcal{M}) = Bm_c r_c(\mathbf{p}_c) \times \mathbb{P}(\hat{W}_c^{(1)} = W_c; \hat{W}_c^{(2)} = W_c)$ $+ Bm_1 r_1(\mathbf{p}_1) \times \mathbb{P}(\hat{W}_{p,1} = W_{p,1})$ $+ Bm_2 r_2(\mathbf{p}_2) \times \mathbb{P}(\hat{W}_{p,2} = W_{p,2})$
	SDMA:	$T_{\text{mcs}}^{\text{SDMA}}(\mathbf{P}, \mathcal{M}) = Bm_1 r_1(\mathbf{p}_1) \times \mathbb{P}(\hat{W}_{p,1} = W_1)$ $+ Bm_2 r_2(\mathbf{p}_2) \times \mathbb{P}(\hat{W}_{p,2} = W_2)$
	NOMA:	$T_{\text{mcs}}^{\text{NOMA}}(\mathbf{P}, \mathcal{M}) = Bm_c r_c(\mathbf{p}_c) \times \mathbb{P}(\hat{W}_c^{(1)} = W_2; \hat{W}_c^{(2)} = W_2)$ $+ Bm_1 r_1(\mathbf{p}_1) \times \mathbb{P}(\hat{W}_{p,1} = W_1)$
MCS-limited sum throughput max. problem (Experiments in this paper)	$OP_{\text{mcs}}^{\text{ma}} : \max_{\mathcal{M}} T_{\text{mcs}}^{\text{ma}}(\mathbf{P}_{\text{wmmse}}^{\text{ma}}, \mathcal{M})$ s.t. $\mathcal{M} \in \mathbb{M}$	

TABLE I: System model differences between RSMA, SDMA and NOMA w.r.t the terminology in Section II-B.

IV. MEASUREMENT RESULTS

In this section, we first describe our measurement campaign in Section IV-A. Then, in Section IV-B, we present measurement results pertaining to $OP_{\text{mcs}}^{\text{ma}}$ with which we compare the measured sum throughput for RSMA, SDMA and NOMA. Then, in Section IV-C, we present a fairness comparison between RSMA, SDMA and NOMA.

A. Measurement campaign

Our measurements were carried out on a lab bench, as shown in Fig. 4. The TX position is fixed along with the

antenna of RX 1, which is placed 0.8m away from the TX⁸. The antenna position of RX 2 is varied as marked in Fig. 4 to create pairs of LoS channels with varying relative strengths and spatial correlation. For NOMA in particular, RX 1 is treated as the strong user and RX 2 the weak user. Every attempt was made to avoid any relative motion between the TXs and RXs during the measurements. For easy reference, a full list of all the parameters relevant to our measurements is provided in Table IV.

To capture the relative pathloss difference between the two channels, we introduce the channel strength disparity

⁸As seen in Table IV, this is the closest TX-RX distance in our experiments. Since it exceeds the Fraunhofer distance, we are operating in the far-field.

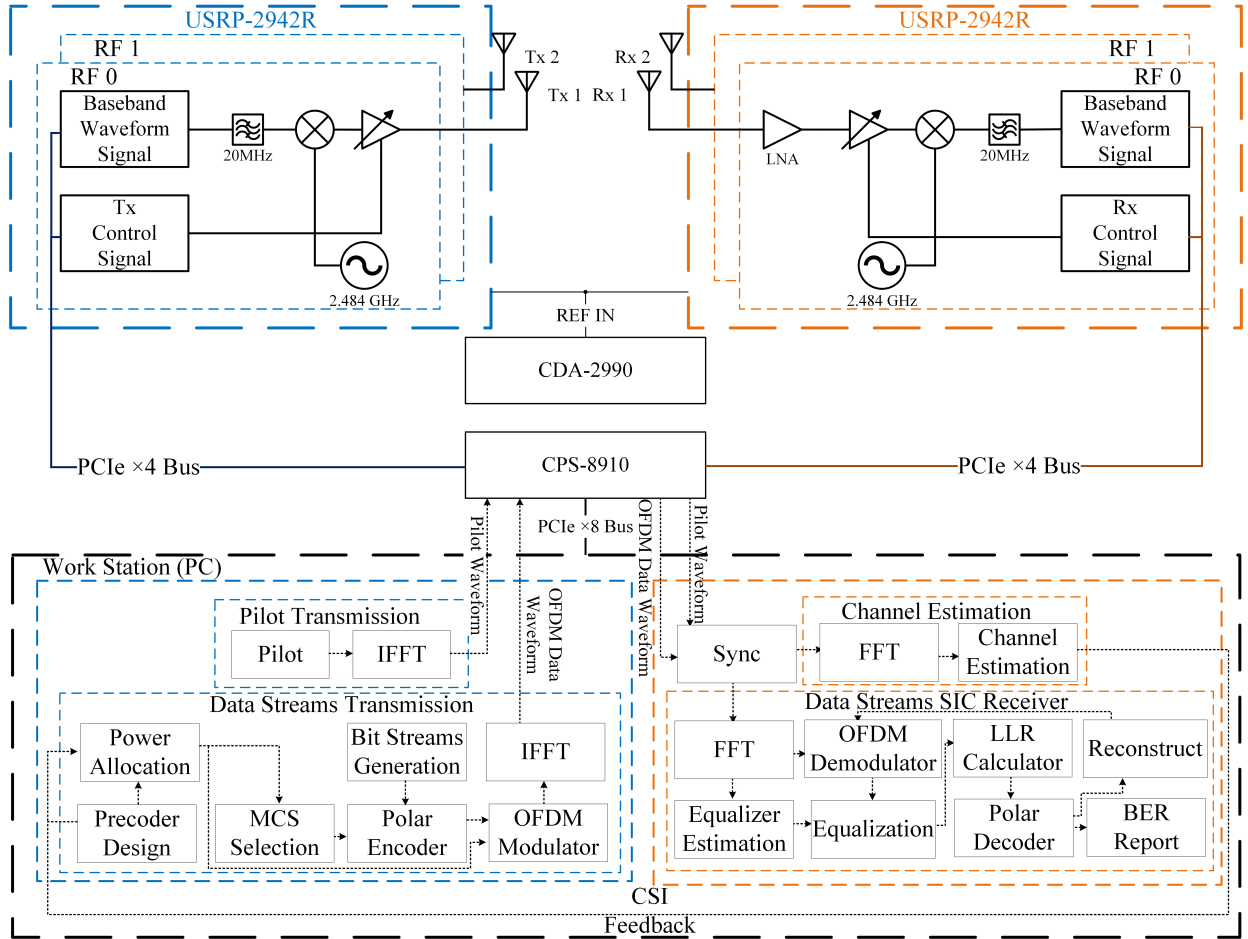


Fig. 2: Block diagram of RSMA Prototype.

No.	Name	Units Description
1.	Workstation	Running LabVIEW NXG
2.	NI USRP-2942	SDRs used to realize TX and RXs
3.	NI CPS-8910	Provides additional PCIe ports
4.	NI CDA-2990	8 Channel, 10 MHz Clock Distribution Device
5.	Linx Technologies ANT-W63WSx	TX antennas
6.	TP-LINK TL-ANT2405C	RX antennas

TABLE II: List of hardware components.

parameter, α , defined in dB scale as follows:

$$\alpha [\text{dB}] = 10 \log_{10} \frac{\|\hat{\mathbf{h}}_2\|}{\|\hat{\mathbf{h}}_1\|}. \quad (18)$$

where $\hat{\mathbf{h}}_i$ ($i = 1, 2$) is given by (1). Hence, RX 2 has a weaker channel when α is negative.

Similarly, to measure the spatial correlation between the two channels, we introduce the correlation parameter, $\rho \in [0, 1]$, defined as follows:

$$\rho = 1 - \frac{|\hat{\mathbf{h}}_1^H \hat{\mathbf{h}}_2|^2}{\|\hat{\mathbf{h}}_1\| \cdot \|\hat{\mathbf{h}}_2\|}. \quad (19)$$

Thus, $\rho = 0$ when the channels are completely aligned, whereas $\rho = 1$ when they are orthogonal.

Based on (18) and (19), we make the following remarks on the cases marked in Fig. 4.

Remark 5. For cases 1 through 3 in Fig. 4, we expect the relative pathloss difference between the two channels to be low by design, as the two RX antennas are fairly close together. In contrast, for cases 4 through 9, RX 2 is much farther from the TX than RX 1; hence, we expect α to be more negative by design. This is validated in Table V, which lists the empirical average of α over all experiment realizations for each case.

Remark 6 (Channels with high spatial correlation). In cases 1, 4 and 7, the channels are expected to be highly spatially correlated (i.e., small ρ) by design, as the two RXs are nearly in a straight line from the TX. This is validated in Table V, which lists the empirical average of ρ over all experiment realizations. RSMA and NOMA are expected to provide large throughput gains over SDMA in these cases, as the common stream allows for the decoding and elimination of interference.

Remark 7 (Channels with low spatial correlation). Similarly,

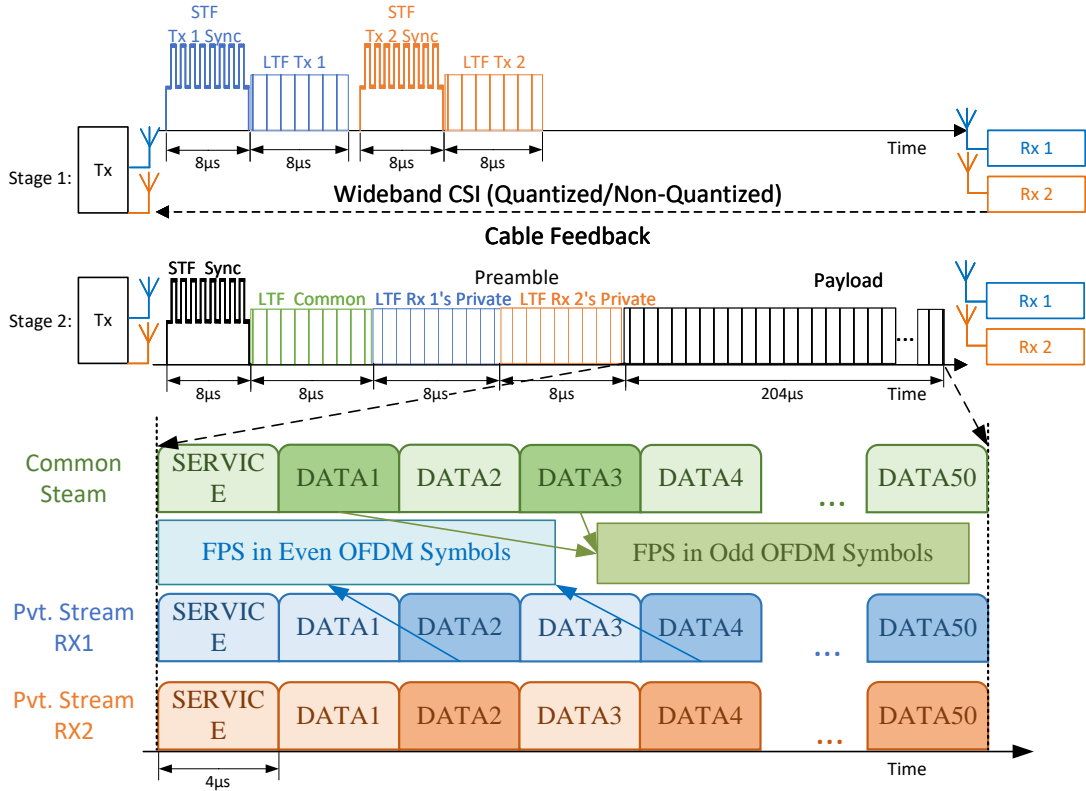


Fig. 3: (Top and middle): The two-stage transmission protocol; (Bottom): OFDM symbol structure within the payload. In conventional 802.11g, every DATA symbol for an RX contains four pilot subcarriers for FPS. However, for RSMA, this approach would cause the pilot subcarriers in the common and private streams to interfere with each other. In particular, the inability to do FPS effectively for the common stream leads to large phase noise. To avoid this, the common (private) stream(s) carry non-zero pilots only in the odd (even) DATA symbols [27].

MCS Index	Modulation (m)	Code Rate, r	Data Rate, Bmr (Mbps)
0	BPSK (1)	1/2	6
1	BPSK (1)	3/4	9
2	QPSK (2)	1/2	12
3	QPSK (2)	3/4	18
4	16QAM (4)	1/2	24
5	16QAM (4)	3/4	36
6	64QAM (6)	2/3	48
7	64QAM (6)	3/4	54
8	256QAM (8)	3/4	72
9	256QAM (8)	5/6	80

TABLE III: MCS levels (largely based on IEEE 802.11g) implemented in our prototype. The data rate in the last column is equal to Bmr , where B is the effective bandwidth given by (14).

in cases 3, 6 and 9, the spatial correlation between the two channels is expected to be relatively low (i.e., larger ρ) by design, due to the larger angular separation between the RXs as seen by the TX. This is validated in Table V. The gain of RSMA over SDMA is expected to be modest, with the common stream being allocated lower power relative to the cases in Remark 6. NOMA is also unlikely to yield significant gains over SDMA; in fact, by forcibly imposing a common stream when the channels are not sufficiently aligned, the NOMA throughput performance can even be worse than SDMA.

B. RSMA v/s SDMA v/s NOMA: Sum Throughput Comparison

As an example measurement, the sum throughput performance for Case 1 as a function of the MCS levels is plotted in Fig. 5 with unquantized CSI feedback. For RSMA/SDMA, the MCS levels for the two private streams are chosen to be identical for ease of illustration⁹. For NOMA, the x -axis corresponds to the MCS of RX 1, as only RX 1 has a private stream. We make the following observations in Fig. 5:

- 1) For a given common stream MCS level for RSMA/NOMA, the sum throughput increases with

⁹Since the two RXs are closely situated for this case, this is also an intuitively good choice. However, in general, the MCS levels of the private streams can be different depending on the channel realizations.

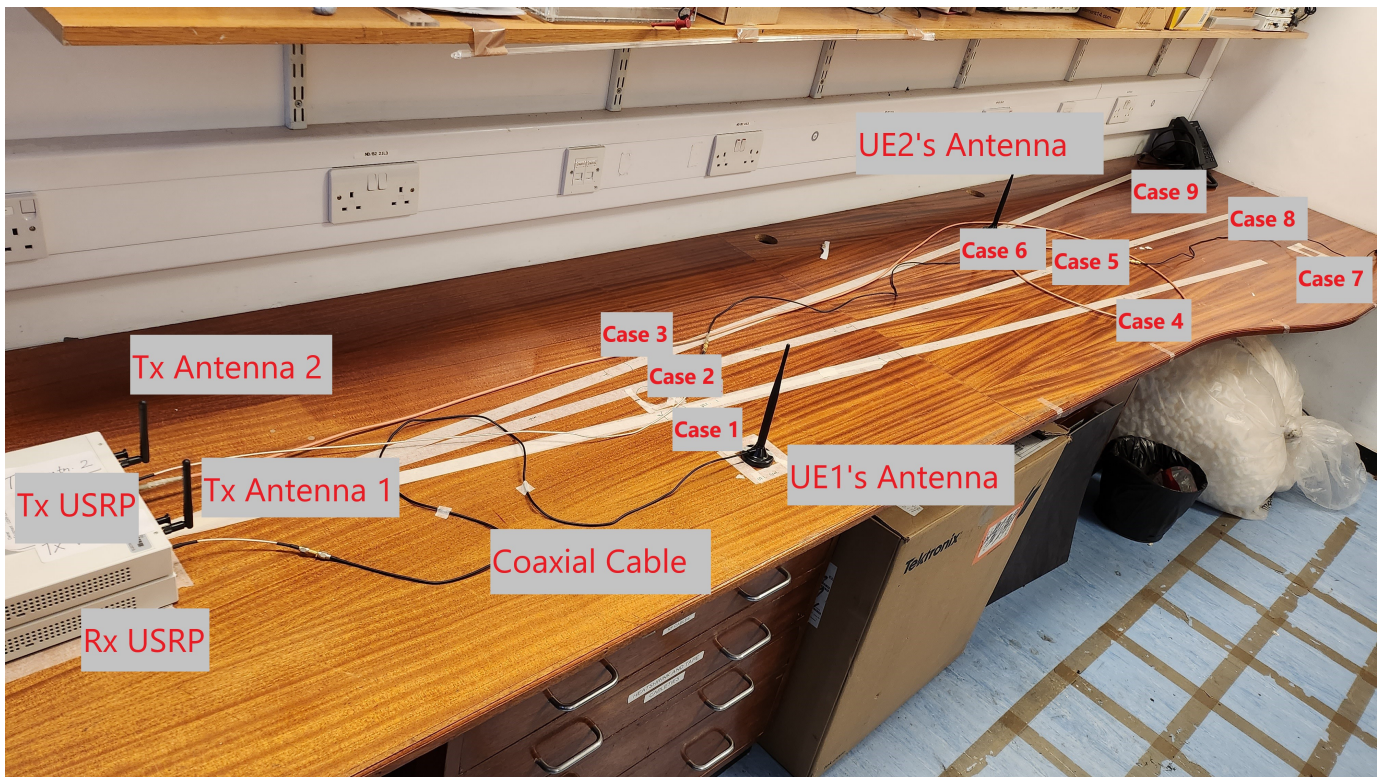


Fig. 4: Layout of measurement cases. The RX antenna positions in the above snapshot correspond to Case 6.

Parameter	Notation (where applicable)	Value
Center frequency	f_c	2.484GHz
Transmit power	P_t	23dBm
TX antenna length		0.13m
Fraunhofer distance		0.28m
Total bandwidth		20MHz
Subcarriers	Total (N_c)	64
	Data	48
	Pilot (FPS)	4
	Guard band	12
CP length		16
Effective bandwidth	B	12MHz
OFDM symbols in payload		50
Experiment runs (per case)		100
Distances	RX 1 \rightarrow TX	0.8m
	RX 2 \rightarrow TX (Cases 1-3)	1.25m
	RX 2 \rightarrow TX (Cases 4-6)	2.10m
	RX 2 \rightarrow TX (cases 7-9)	3.30m
Channel coding		Polar codes
List depth		2
Environment		LoS

TABLE IV: List of parameters used in our experiments.

the private stream MCS level up to a point as expected, before dropping when the MCS level is too aggressive. The same behavior is observed for SDMA as well, which does not have a common stream.

- For a given private stream MCS level, a similar trend as above can also be seen w.r.t common stream MCS level for RSMA/NOMA. Specifically, the RSMA/NOMA sum throughput increases as the common stream MCS level is raised from QPSK rate 1/2 (MCS index 2 in Table III) to 16QAM rate 3/4 (MCS index 5 in Table III). However, the very next MCS level of 64QAM rate 3/4 for the

	Relative pathloss		Spatial correlation	
	Cases	α [dB]	Cases	ρ
Low	1	-7.6	1	0.15
	2	-6.4	4	0.16
	3	-8.8	7	0.24
Medium	4	-14.5	2	0.48
	5	-13.0	5	0.46
	6	-13.0	8	0.35
High	7	-23.6	3	0.95
	8	-24.7	6	0.95
	9	-22.1	9	0.85

TABLE V: The cases marked in Fig. 4 correspond to pairs of channels that vary in terms of their relative pathloss and spatial correlation, captured by α and ρ defined in (18) and (19), respectively. The above table lists the empirical average of α and ρ over all experiment realizations for each case.

common stream is too aggressive and due to the resulting error propagation, the RSMA/NOMA sum throughput is lower than SDMA. To demonstrate this, Fig. 6 shows the superposed received symbol constellation for RSMA at RX 1, corresponding to the MCS levels marked by points 'C' and 'A' in Fig. 5. The MCS levels at point C being conservative, a QPSK constellation (private stream) superposed on another QPSK constellation (common stream) is clearly visible in Fig. 6a. In a similar vein, if the MCS levels at point A were *not* aggressive, then we would expect to see 256 distinct symbol clusters in Fig. 6b, corresponding to a superposition of 64QAM (common stream) and QPSK (private stream) constellations. However, we only observe 81 distinct symbol

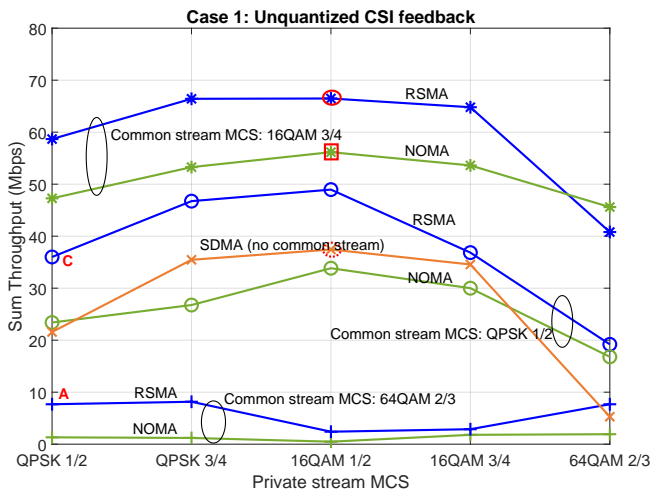


Fig. 5: For Case 1, the large spatial correlation (i.e., small ρ , see Table V) between the RX channels induces high mutual interference. Under these conditions, RSMA and NOMA can achieve significant throughput gains over SDMA with the help of the common stream, provided its MCS level is not too aggressive. The highest measured sum throughput above are: 66.48Mbps for RSMA, 56.16Mbps for NOMA, and 37.44Mbps for SDMA.

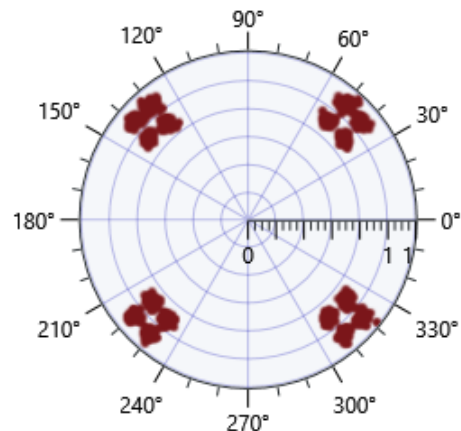
clusters, which leads to high error rates for the common stream.

- 3) Points 1 and 2 above highlight the role of MCS selection in realizing sum throughput gains for RSMA and NOMA over SDMA. The highest measured sum throughput in Fig. 5 is the empirical solution to OP_{mcs}^{ma} in Table I, with the additional constraint that the MCS levels for the two private streams in RSMA/SDMA are identical. For RSMA, this value is equal to 66.48Mbps (marked with a solid red circle); for NOMA, it is equal to 56.16Mbps (red square), and for SDMA it is only 37.44Mbps (dashed red circle).
- 4) Finally, for all data points bar one, the RSMA sum throughput exceeds that of NOMA. Since RX 2's channel is not much weaker than RX 1 for Case 1 (see α in Table V), RSMA provides additional throughput gain through the private stream of RX 2.

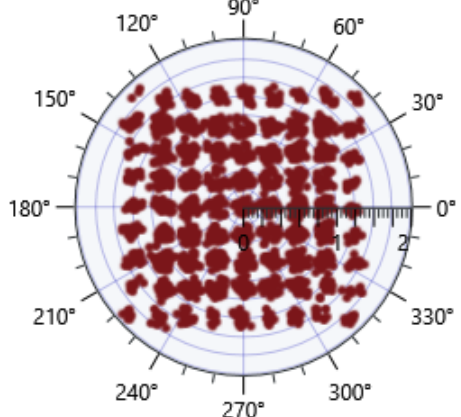
Fig. 7 plots the empirical solution for OP_{mcs}^{ma} , broken down in terms of the contributions of the common and private streams. We make the following observations:

A. Unquantized CSI feedback:

- 1) As expected for RSMA, the contribution of the common stream (green bars) diminishes with increasing ρ (Remarks 6 and 7); in particular, for cases 1, 4 and 7, the common stream constitutes 51%, 62% and 62% of the sum throughput, respectively, whereas for cases 3, 6 and 9, this drops to 22%, 34% and 17%, respectively.
- 2) In cases 1, 4 and 7, where the channels have high spatial correlation (low ρ , see Table V), SDMA's sum throughput is significantly lower than those of RSMA and NOMA due to the high mutual inter-



(a) Common stream: QPSK 1/2, private stream: QPSK 1/2



(b) Common stream: 64-QAM 2/3, private stream: QPSK 1/2

Fig. 6: Superposed received symbol constellation for RSMA at RX 1 for the MCS levels in Fig. 5 corresponding to: (a) point 'C', which is an example of a conservative choice of MCS levels. Hence, the superposition of QPSK and QPSK constellations is clearly visible; (b) point 'A', which is an aggressive choice of MCS for the common stream. Instead of 256 distinct symbol clusters due to a superposition of 64-QAM and QPSK constellations, we only observe 81 distinct symbol clusters, which leads to high error rates for the common stream.

ference. The gains of RSMA and NOMA in these cases stem from the decoding and elimination of interference through the common stream (Remark 6). In particular, RSMA achieves gains of 82%, 103% and 134%, respectively, over SDMA as shown by the up arrows in Fig. 7). On the other hand, RSMA's gain over NOMA for these cases is quite modest (23% for Case 1, none for Case 4 and 19% for Case 7).

- 3) In cases 3, 6 and 9, where the channels have low spatial correlation (high ρ , see Table V), RSMA's gain over SDMA is modest due to the relatively lower mutual interference. On the other hand, the NOMA sum throughput is significantly worse than both RSMA and SDMA. In particular, RSMA achieves gains of 38%, 45%, and 19%, respectively, for these three cases over NOMA.

B. Quantized CSI feedback:

- 1) Unsurprisingly, all three multiple access schemes experience a sum throughput loss due to CSI quantization. However, SDMA and RSMA are more adversely affected than NOMA, especially in cases 4 through 9, where there is a significant pathloss difference between the two channels. For these cases, most of the throughput loss for RSMA and SDMA can be attributed to the private stream of RX 2 – the weaker user. In contrast, the robustness of NOMA to CSI quantization stems from the fact that RX 2 does not have a private stream. Furthermore, due to the very low private stream throughput for RX 2, the RSMA throughput performance is similar to NOMA for these cases.
- 2) However, in the absence of a large pathloss difference between the two channels – for instance, in cases 2 and 3 – the private stream throughput for RX 2 is still quite high, despite the loss from CSI quantization. Under these conditions, NOMA with its missing private stream for RX 2 continues to perform worse than both RSMA and SDMA, mirroring the performance seen with unquantized CSI feedback.
- 3) In all cases bar one, RSMA’s gain over SDMA is much larger when compared to unquantized CSI feedback. This is because imperfect CSI has a more adverse effect on private stream throughputs due to the higher residual interference. Thus, due to the throughput contribution of the common stream, which stays pretty steady even with quantized CSI, RSMA’s throughput loss is lower than that of SDMA.

In summary, RSMA achieves the best throughput performance across (a) different RX channels that vary in their relative strength and spatial correlation, and (b) different CSI quality. In some cases, SDMA is effective while in others NOMA is effective. RSMA is effective in all the cases, and thus effectively bridges between both SDMA and NOMA.

C. RSMA v/s SDMA v/s NOMA: Fairness Comparison

In the previous subsection, we saw that for RSMA, the private stream throughput of RX 2 is severely diminished when there is a large pathloss difference between the two channels and imperfect CSI (bullet point B1). To increase RX 2’s total throughput in such cases, a larger fraction (> 0.5) of the common stream can be allocated to it. This would not alter the RSMA sum throughput¹⁰, but would achieve better (max-min) fairness [17].

In this subsection, we experimentally verify this possibility of improved fairness afforded by RSMA. This is done in the following manner for each case in Fig. 7:

- S1) if $R_1(\mathbf{P}_{\text{wmmse}}^{\text{RSMA}}) - R_2(\mathbf{P}_{\text{wmmse}}^{\text{RSMA}}) \leq R_c(\mathbf{P}_{\text{wmmse}}^{\text{RSMA}})$, then the common stream is partitioned such that $R_1(\mathbf{P}_{\text{wmmse}}^{\text{RSMA}}) + (W_{c,1}/W_c)R_c(\mathbf{P}_{\text{wmmse}}^{\text{RSMA}}) =$

- $R_2(\mathbf{P}_{\text{wmmse}}^{\text{RSMA}}) + (W_{c,2}/W_c)R_c(\mathbf{P}_{\text{wmmse}}^{\text{RSMA}})$ to ensure that both RXs have the same throughput;
 S2) otherwise, when $R_1(\mathbf{P}_{\text{wmmse}}^{\text{RSMA}}) - R_2(\mathbf{P}_{\text{wmmse}}^{\text{RSMA}}) > R_c(\mathbf{P}_{\text{wmmse}}^{\text{RSMA}})$, the entire common stream is allocated to RX 2. This is similar to NOMA, albeit RX 2 has a private stream as well.

Remark 8 (Fairness while maximizing throughput). *User fairness in RSMA/SDMA/NOMA is often framed as an optimization problem, where the objective is to maximize the minimum user throughput through precoder design. Hence, the optimal precoders for fairness are, in general, different from the optimal precoders for sum throughput maximization. The fairness strategy in S1 and S2 differs from this viewpoint by trying to achieve fairness without changing the precoders. In other words, we are trying to achieve fairness while still maximizing the sum throughput. This ability to realize both objectives simultaneously is a unique feature of RSMA. S1 and S2 cannot be realized for NOMA and SDMA because the former does not have a private stream for RX 2 and the latter does not have a common stream.*

Fig. 8 compares the relationship between the sum throughput and the minimum throughput for RSMA (subject to S1 and S2), SDMA and NOMA. The case number is indicated beside each data point in the same color. The dashed $y = 2x$ line represents max-min fairness and the region above it is feasible for all three multiple access schemes. Thus, points that are closer (in terms of Euclidean distance) to the dashed line represent *fairer* outcomes. Based on this insight, we make the following remarks:

- When S1 is true, the corresponding RSMA point lies on the dashed line (i.e., achieves max-min fairness), as seen for all cases bar one in Figs. 8a and b. Otherwise, for S2, the RSMA point lies *as close as possible* above the dashed line, as seen for case 8 in Figs. 8a and b.
- In Fig. 8a, SDMA also achieves approximate fairness for some cases (namely 1, 2, 3 and 4), as does NOMA (case 7). However, the RSMA points achieve fairness at a higher sum for these cases lie to the *northeast* of the corresponding SDMA/NOMA points, which indicates fairness at a higher sum throughput.

In summary, RSMA is capable of achieving better fairness at a higher sum throughput than both SDMA and NOMA, regardless of CSI quality, through a judicious allocation of the common stream to the weaker RX.

V. SUMMARY

In this paper, we realized the first-ever RSMA prototype using SDRs in order to experimentally validate its performance gains promised in the theoretical literature. To this effect, we measured the throughput and fairness performance of RSMA, SDMA and NOMA using our prototype for the two-user MISO scenario over (a) different pairs of channels varying in terms of their relative strength and spatial correlation and (b) different CSI quality. Across these different cases, we observed that RSMA achieved the highest sum throughput, whereas SDMA and NOMA were each effective only in some cases.

¹⁰For precisely this reason, the allocation of the common stream between the two RXs is not mentioned when discussing the sum throughput results in Section IV-B.

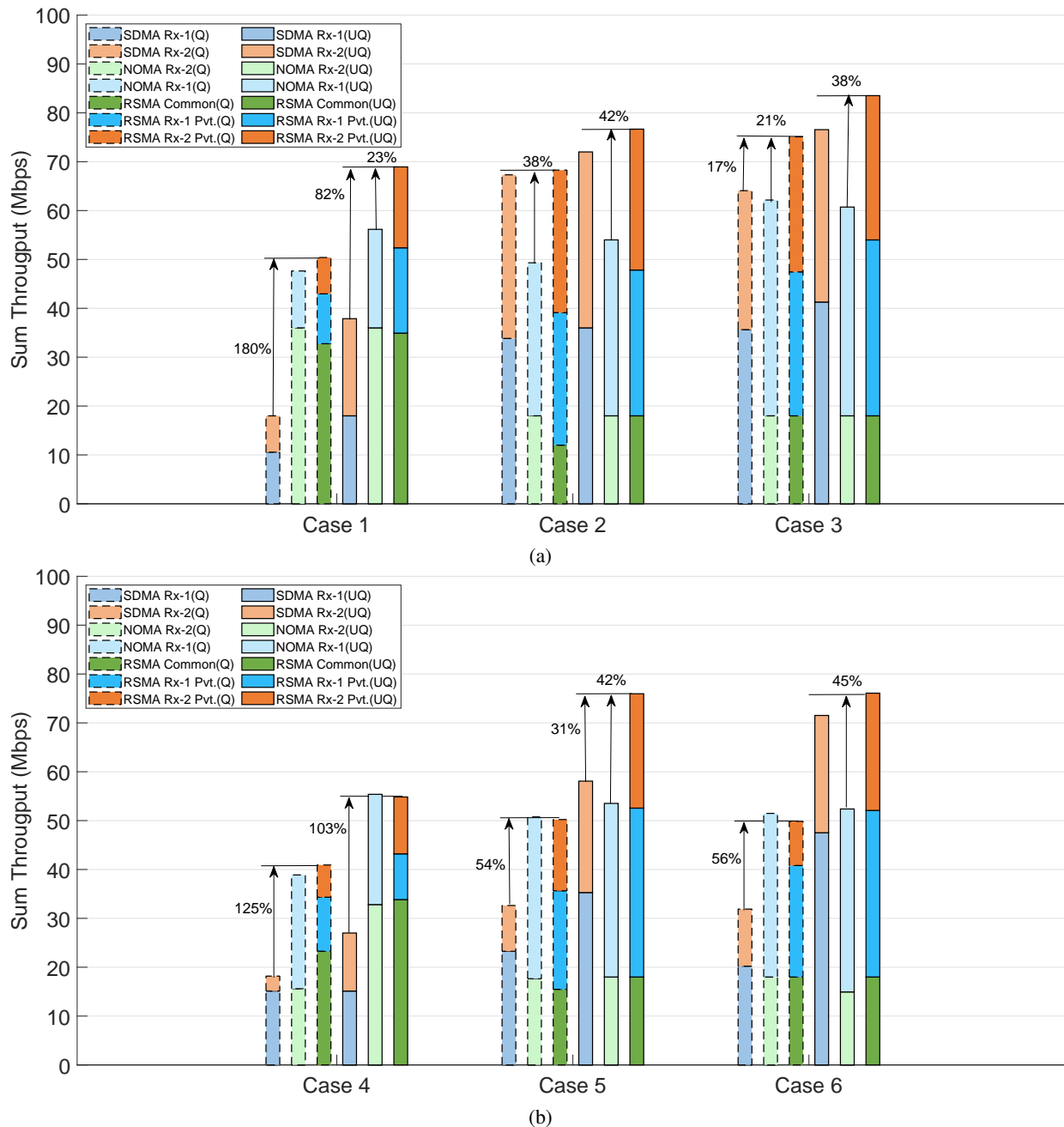


Fig. 7: The maximum measured sum throughput under unquantized (UQ) and quantized (Q) CSI feedback for RSMA, SDMA and NOMA, which correspond to the empirical solutions of OP_{mcs}^{RSMA} , OP_{mcs}^{SDMA} and OP_{mcs}^{NOMA} , respectively. The arrows indicate RSMA's gain w.r.t. SDMA and NOMA.

We also observed that RSMA achieved better fairness at a higher sum throughput than both SDMA and NOMA. As the first-ever experimental comparison between RSMA, SDMA and NOMA, our efforts in this paper address the pressing question of which multiple access technique is best equipped to deliver the performance enhancements expected from next-generation networks like 6G. Thus, the superior performance of RSMA in these experiments provides the impetus for further experimental efforts at a larger scale and in more challenging operating environments.

ACKNOWLEDGMENTS

We thank Onur Dizdar for his valuable inputs on Polar code implementation.

APPENDIX A CSI QUANTIZATION TECHNIQUE

The quantized wideband CSI, $\hat{\mathbf{h}}_i^Q := [\hat{h}_{i1}^Q \ \hat{h}_{i2}^Q]$, is obtained from $\hat{\mathbf{h}}_i = [\hat{h}_{i1} \ \hat{h}_{i2}]$, as follows:

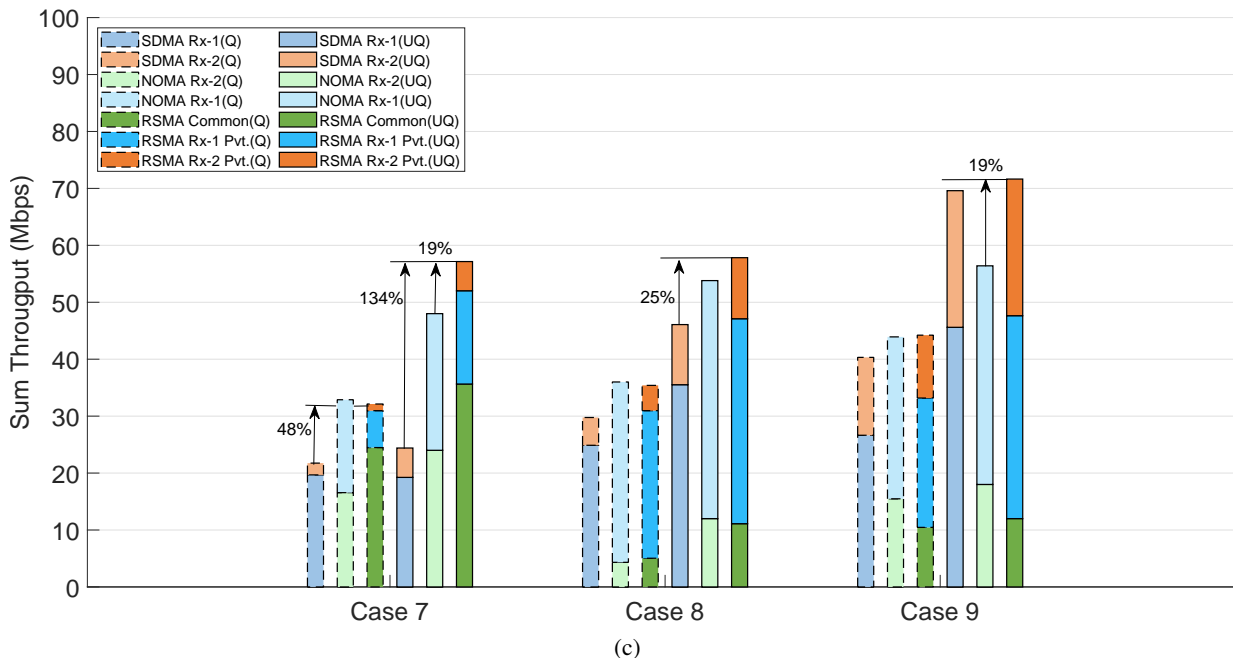


Fig. 7: (contd.)

(a) The *linear scaler* is evaluated as follows:

$$M_h^{\text{lin}} := \frac{m_h}{10^{M_h/20}} \quad (20)$$

$$\text{where } m_h := \max_{i,l} \{ |\text{Re}(\hat{h}_{il})|, |\text{Im}(\hat{h}_{il})| \} \quad (i, l \in \{1, 2\}), \quad (21)$$

$$\text{and } M_h := \min \left\{ 7, \left\lfloor 20 \log_{10}(m_h) \right\rfloor \right\}. \quad (22)$$

M_h in (22) is known as the scaling ratio and is quantized to three bits for feedback.

(b) Using (20), the real and imaginary parts \hat{h}_{ij} are quantized using $N_b = 4$ bits in our prototype as follows.

$$\text{Re}(\hat{h}_{ij}^{\text{Q}}) := \text{round} \left(\frac{\text{Re}(\hat{h}_{ij})}{M_h^{\text{lin}}} (2^{N_b-1} - 1) \right) \quad (23)$$

$$\text{Im}(\hat{h}_{ij}^{\text{Q}}) := \text{round} \left(\frac{\text{Im}(\hat{h}_{ij})}{M_h^{\text{lin}}} (2^{N_b-1} - 1) \right) \quad (24)$$

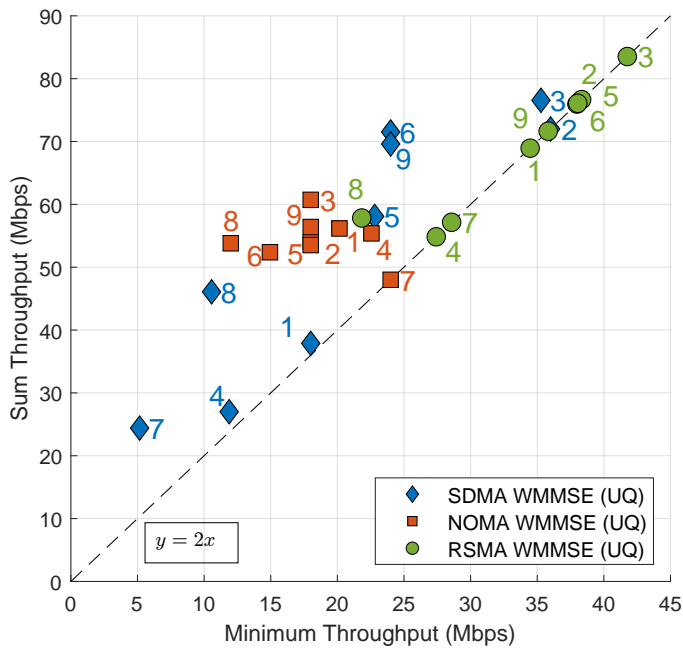
The feedback overhead for the entire CSI equals $3 + 2N_b il$ bits, where the first term corresponds to the scaling ratio, and the factor of two in the second term accounts for the real and imaginary parts of \hat{h}_{ij}^{Q} . For our prototype, this value equals 35 bits, as opposed to the $128il = 512$ bits without quantization.

At the TX, the CSI estimates, denoted by \hat{h}_{il}^{TX} , are recovered as follows:

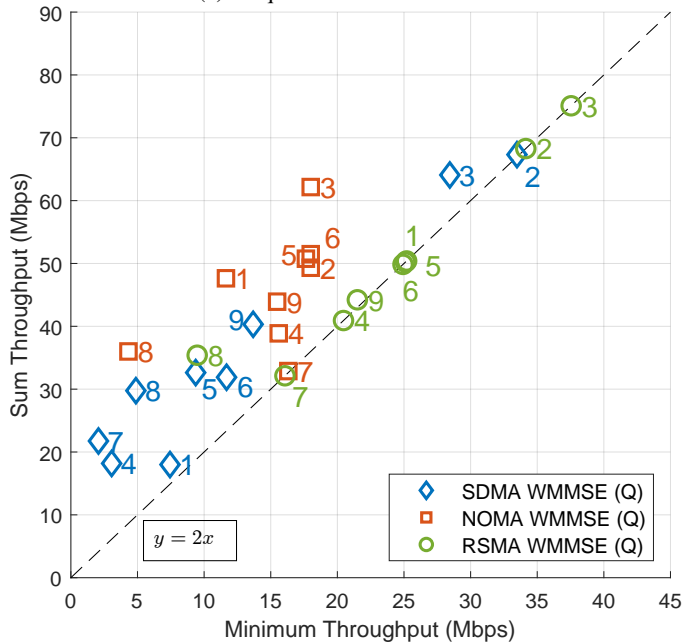
$$\hat{h}_{il}^{\text{TX}} := \frac{\hat{h}_{il}^{\text{Q}}}{10^{M_h/20}} \quad (i, l \in \{1, 2\}). \quad (25)$$

REFERENCES

- [1] "6G: The next hyper - connected experience for all," White paper, Samsung Research. [Online]. Available: <https://cdn.codeground.org/nsr/downloads/researchareas/6G%20Vision.pdf>
- [2] T. Cover, "Broadcast channels," *IEEE Trans. Inf. Theory*, vol. 18, no. 1, pp. 2–14, 1972.
- [3] S. M. R. Islam, N. Avazov, O. A. Dobre, and K.-s. Kwak, "Power-domain non-orthogonal multiple access (NOMA) in 5G systems: Potentials and challenges," *IEEE Commun. Surveys Tuts.*, vol. 19, no. 2, pp. 721–742, 2017.
- [4] Y. Saito *et al.*, "Non-orthogonal Multiple Access (NOMA) for cellular future radio access," in *2013 IEEE 77th Vehicular Technology Conference (VTC Spring)*, 2013, pp. 1–5.
- [5] V.-D. Nguyen *et al.*, "Precoder design for signal superposition in MIMO-NOMA multicell networks," *IEEE J. Sel. Areas Commun.*, vol. 35, no. 12, pp. 2681–2695, 2017.
- [6] S. Timotheou and I. Krikidis, "Fairness for Non-Orthogonal Multiple Access in 5G systems," *IEEE Signal Process. Lett.*, vol. 22, no. 10, pp. 1647–1651, 2015.
- [7] Z. Ding *et al.*, "Application of Non-Orthogonal Multiple Access in LTE and 5G networks," *IEEE Commun. Mag.*, vol. 55, no. 2, pp. 185–191, 2017.
- [8] B. Clerckx *et al.*, "Is NOMA efficient in multi-antenna networks? A critical look at next generation multiple access techniques," *IEEE Open Journal of the Communications Society*, vol. 2, pp. 1310–1343, 2021.
- [9] Q. Spencer, A. Swindlehurst, and M. Haardt, "Zero-forcing methods for downlink spatial multiplexing in multi-user MIMO channels," *IEEE Trans. Signal Process.*, vol. 52, no. 2, pp. 461–471, 2004.
- [10] Y. Mao, B. Clerckx, and V. O. Li, "Rate-Splitting Multiple Access for Downlink Communication Systems: Bridging, Generalizing, and Outperforming SDMA and NOMA," *EURASIP Journal on Wireless Communications and Networking*, vol. 2018, no. 1, p. 133, May 2018.
- [11] Y. Liu *et al.*, "Multiple-antenna-assisted non-orthogonal multiple access," *IEEE Wireless Commun.*, vol. 25, no. 2, pp. 17–23, 2018.
- [12] Y. Qi, X. Zhang, and M. Vaezi, "Over-the-air implementation of NOMA: New experiments and future directions," *IEEE Access*, vol. 9, pp. 135 828–135 844, 2021.
- [13] A. Benjebbour *et al.*, "Non-orthogonal multiple access (NOMA): Concept, performance evaluation and experimental trials," in *Proc. of the Intl. Conf. on Wireless Networks and Mobile Communications (WINCOM)*, 2015, pp. 1–6.
- [14] —, "Outdoor experimental trials of advanced downlink NOMA using smartphone-sized devices," in *Proc. of the 87th IEEE Vehicular Tech. Conf. (VTC Spring)*, 2018, pp. 1–6.
- [15] A. Benjebbour and Y. Kishiyama, "Combination of NOMA and MIMO: Concept and experimental trials," in *Proc. of the 25th Intl. Conf. on Telecommunications (ICT)*, 2018, pp. 433–438.
- [16] H. Joudeh and B. Clerckx, "Sum-rate maximization for linearly precoded downlink multiuser MISO systems with partial CSIT: A rate-splitting approach," *IEEE Trans. Commun.*, vol. 64, no. 11, pp. 4847–4861, 2016.



(a) Unquantized CSI feedback



(b) Quantized CSI feedback

Fig. 8: Fairness comparison between RSMA (subject to S1 and S2), SDMA and NOMA. The number beside each data point indicates the measurement case from Fig. 4. The dashed line ($y = 2x$) corresponds to max-min fairness and points that are closer (in terms of Euclidean distance) to this line represent fairer outcomes.

[17] Y. Mao *et al.*, “Rate-Splitting Multiple Access: Fundamentals, Survey, and Future Research Trends,” *IEEE Commun. Surveys Tuts.*, 2022.

[18] B. Clerckx *et al.*, “A Primer on Rate-Splitting Multiple Access: Tutorial, Myths, and Frequently Asked Questions,” *IEEE J. Sel. Areas Commun.*, vol. 41, no. 5, pp. 1265–1308, May 2023.

[19] B. Clerckx, Y. Mao, R. Schober, and H. V. Poor, “Rate-Splitting Unifying SDMA, OMA, NOMA, and Multicasting in MISO Broadcast Channel: A Simple Two-User Rate Analysis,” *IEEE Wireless Commun. Lett.*, vol. 9, no. 3, pp. 349–353, 2020.

[20] O. Dizdar, Y. Mao, W. Han, and B. Clerckx, “Rate-Splitting Multiple Access for Downlink Multi-Antenna Communications: Physical Layer Design and Link-level Simulations,” in *Proc. of the 31st Annual IEEE Intl. Symp. on Personal, Indoor and Mobile Radio Communications (PIMRC)*, Aug. 2020.

[21] H. Chen *et al.*, “Link-Level Performance of Rate-Splitting based Downlink Multiuser MISO systems,” in *Proc. of the 31st Annual IEEE Intl. Symp. on Personal, Indoor and Mobile Radio Communications (PIMRC)*, Aug. 2020.

[22] S. Zhang *et al.*, “Rate-splitting multiple access: Finite constellations, receiver design, and SIC-free implementation,” 2023.

[23] C. Mosquera and F. Gómez-Cuba, “Link Adaptation for Rate Splitting Systems with partial CSIT,” *IEEE J. Sel. Areas Commun.*, vol. 41, no. 5, pp. 1336–1350, May 2023.

[24] Y. Wang, V. W. S. Wong, and J. Wang, “Flexible Rate-Splitting Multiple Access with Finite Blocklength,” *IEEE J. Sel. Areas Commun.*, vol. 41, no. 5, pp. 1398–1412, May 2023.

[25] “IEEE Std. 802.11n-2009,” Technical Standards, IEEE Standard for Information technology – Local and metropolitan area networks – Specific requirements– Part 11: Wireless LAN Medium Access Control (MAC) and Physical Layer (PHY) Specifications Amendment 5: Enhancements for Higher Throughput.

[26] S. S. Christensen, R. Agarwal, E. De Carvalho, and J. M. Cioffi, “Weighted sum-rate maximization using weighted mmse for mimo-bc beamforming design,” *IEEE Trans. Wireless Commun.*, vol. 7, no. 12, pp. 4792–4799, Dec. 2008.

[27] R. Zlobin, A. Kureev, and E. Khorov, “Receiver Design and Frame Format for Uplink NOMA in Wi-Fi,” in *Proc. of the IEEE INFOCOM Workshops*, 2022, pp. 1–2.

[28] H. Minn, “A robust timing and frequency synchronization for OFDM systems,” *IEEE Trans. Wireless Commun.*, vol. 2, no. 4, pp. 822–839, 2003.

[29] P. Trifonov, “Efficient Design and Decoding of Polar Codes,” *IEEE Trans. Commun.*, vol. 60, no. 11, pp. 3221–3227, 2012.

[30] H. Li and J. Yuan, “A Practical Construction Method for Polar Codes in AWGN Channels,” in *IEEE 2013 Tencon - Spring*, 2013, pp. 223–226.

[31] I. Tal and A. Vardy, “List Decoding of Polar Codes,” *IEEE Trans. Inf. Theory*, vol. 61, no. 5, pp. 2213–2226, 2015.